Acta of Bioengineering and Biomechanics
Vol. 19, No. 4, 2017

Original paper
DOI: 10.5277/ABB-00876-2017-03

Synthesizing and characterization of nano-Graphene Oxide-reinforced Hydroxyapatite Coatings on laser treated Ti6Al4V surfaces

ERTUĞRUL BULBUL, BUNYAMIN AKSAKAL*

Faculty of Chemistry and Metallurgy, Department of Metallurgy and Materials Engineering,
Yildiz Technical University, Istanbul, Turkey.

Laser-treated Ti6Al4V surfaces were coated by the single-layer hydroxyapatite (HA) and double-layer hydroxyapatite reinforced by the reduced nano-graphene oxide (rGO) using the sol-gel method. The effects of rGO reinforcement at different ratios and sintering temperatures on surface morphology and adhesion strength of the single and double layer coatings (rGO/HA) were analysed. As the initial treatment process, a laser texturing was patterned on the alloy and then, prepared samples were coated. The coated laser-modified HA and HA/rGO-coated Ti6Al4V surfaces were characterized by Raman spectroscopy, X-ray diffraction (XRD), Field Emission Scanning Electron Microscope (FESEM) and the adhesion strength between the coat and substrates were determined by the standard adhesion tests. The conducted analyses indicated that the substitution of rGO into HA matrix revealed a homogeneous morphology and relatively crack-free coatings on the laser-treated Ti substrate surfaces. Adhesion tests showed that, the HA + rGO (1.0 wt. %) biocomposites exhibited a significant increase in adhesion strength compared to untreated surfaces and to the single HA-coated Ti6Al4V substrates.

Key words: *surface treatment, hydroxyapatite, nano-graphene oxide, sol-gel*

1. Introduction

Due to the intrinsic properties of high coherence and directionality, the laser treatment can be applied on metallic surfaces to perform a broad range of treatments, such as remelting, alloying and cladding, which are used to improve the wear and corrosion resistance of titanium alloys [22]. The disadvantages of titanium alloys can be compansated by laser surface modification treatment coupled with other bioceramic coatings such as hydroxyapatite, $Ca_{10}(PO_4)_6OH_2$ (HA) and graphene. However, some shortcomings such as brittleness, low wear resistance, and low fracture toughness still limit the use of HA in load-bearing and long-term implant applications [5], [18]. Mechanical performance of HA can be improved by incorporating second phase reinforcements such as graphene and other carbonaceous materials [2]–[7]. Previously, carbon nano-materials such as carbon nano-tubes and graphene nano-sheets have found wide acceptance as fillers in ceramic matrices due to their high mechanical properties such as Young's modulus (up to 1 TPa) and intrinsic strength (approx. 130 GPa) [26], [5].

Graphene, having the monolayer of sp^2-hybridized carbon atoms arranged in a two-dimensional lattice, has excellent mechanical, thermal and electronic properties is now expanding its territory beyond electronic and chemical applications toward biomedical areas [10], [6], [22]. In addition, due to its hydrophobicity and high specific surface area of inherent to its two-dimensional lattice geometry, and its excellent aqueous processibility, mechanical strength (Young's

* Corresponding author: Bunyamin Aksakal, Department of Metallurgy and Materials Engineering, Faculty of Chemistry and Metallurgy, Yildiz Technical University, 2334 Istanbul, Turkey. Phone: +90 212 383 4662, e-mail: baksakal2@gmail.com

Received: March 15th, 2017
Accepted for publication: April 27th, 2017

modulus, ~1.1 TPa) and intrinsic bio-compatibility are considered as a promising material for biological applications [13]. Moreover, the reactive oxygenic groups, present on the edges (carbonyl and carboxyl groups) and planes (hydroxyl and epoxide groups) of rGO sheets can stabilize the dispersion of rGO in aqueous media, enhance the interfacial bonding within the components, and facilitate the stress transfer in the composites which render rGO as attractive and promising nanoscale reinforcement. The Graphene--based chitosan biocomposites displayed a significant improvement in tensile strength and Young's modulus when containing the addition of graphene [24], [20], [21], [16].

It was also reported that graphene oxide (GO) can improve the properties of HA due to its good biocompatibility and excellent mechanical properties [14]. Additionally, GO showed inhibition effect of bacterial growth on the surfaces [27]. It was also reported that a combination of HA with GO, the surface properties of hosting material may also play an important role for biomaterials for long term benefits [13]. Such benefits depend upon the responses of the surrounding host tissues, regarding integration, formation of a connection between the living bone and the surface of load-carrying implants [25]. Few surface modifications such as bioceramic coatings on sand blasted and laser--treated surface modification are also the most promising methods for metallic surfaces to produce high surface area [25], [8].

This paper presents two different novel coatings on the laser-treated Ti6Al4V surfaces. The laser-treated Ti samples were coated both by single HA- and rGO-reinforced (0.5 and 1.0%) HA at different sintering temperatures, e.g., 750, 800 and 850 °C.

2. Materials and methods

2.1. Material

Titanium alloy (Ti6Al4V) was used in the form of sheet material (Timed, Inc., Turkey) and the elemental composition was given in Table 1. Ti6Al4V substrate sheets were initially machined to 2×10×15 mm, ultrasonically cleaned in isopropanol and dried. Before the laser treatment, prepared specimens were cleaned ultrasonically in a distilled water, then rinsed in pure distilled water and, finally, in absolute ethanol. The samples then were ultrasonically cleaned with deionized water, in acetone and ethanol and were passivated in HNO_3 (25%) solution. Then they were ultrasonically cleaned again with deionized water for 30 min and then dried at room temperature. Hydroxyapatite (Merck, 25 μm) and the synthesized rGO (~200 nm) powders were used in coating of the laser treated Ti6Al4V substrates.

2.2. Laser processing

Laser surface texturing (LST) is a progress for surface modification of metals and ceramics. In the present investigation, Ti-6Al-4V samples (Grade 5) were prepared with a dimension of 2×15×10 mm and mechanically polished for LST process. Initially all samples were prepared with the standard specimen cleaning techniques, cleaned in ultrasonic bath (400 W) and dried in a vacuum oven. All surface processes were carried out with the laser beam and samples were initially investigated by optic microscope and surface pattern was determined. After that, the laser process was preceded as initially, determining the penetration depth of the material. Pattern types were determined (Fig. 2) before the process with the widths (2 μm) and depths (2 μm). Afterwards, the targets were irradiated at normal incidence using a laser beam by using Fiber source (Yb). The laser beam irradiated the target at an incident angle of 90° and the system also ensured that the target was carefully positioned in the lens focal plane (z-axis). Laser treatment of the samples was carried out using a Fiber Laser (F40S, Laser Sos, Istanbul, Turkey). This fiber laser system was utilized due to its versatility, high unsaturated gain and mostly high-power output capabilities. A continuous wave laser operation was implemented with a maximum power output of 40 kW (1–1000 kHz frequency, focal point 163 mm ± 2 mm) at a wavelength of 1060 nm. The irradiation was carried out in air at atmospheric pressure and standard relative humidity accordingly to the schematics shown in Fig. 1.

Table 1. Chemical composition of Ti-6Al-4V alloy

wt. %	Ti	C	Fe	N	Al	O	V	H	Y
Ti-6Al-4V	bal	0.08	0.03	0.05	5.5–6.75	0.20	3.5–4.5	0.015	0.005

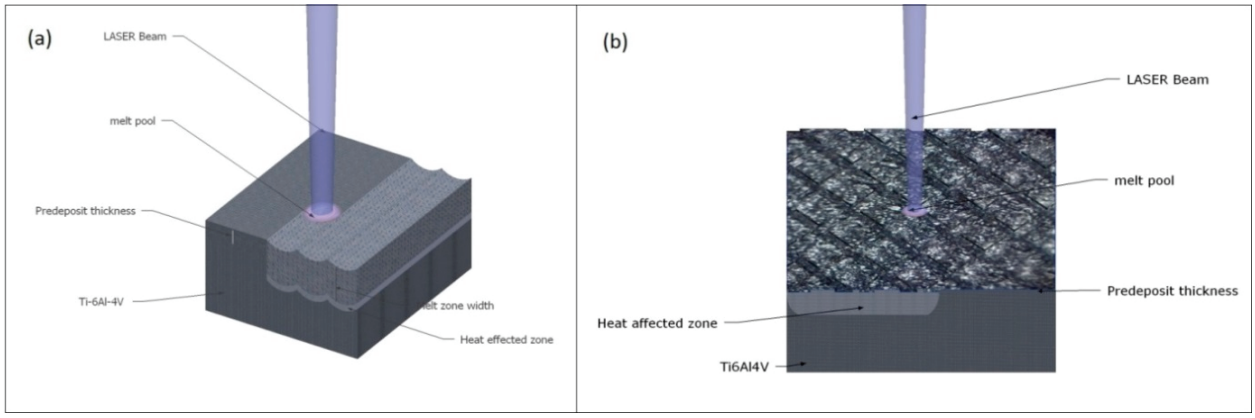

Fig. 1. Schematic representation of laser surface processes: (a) surface modification, (b) surface texturing

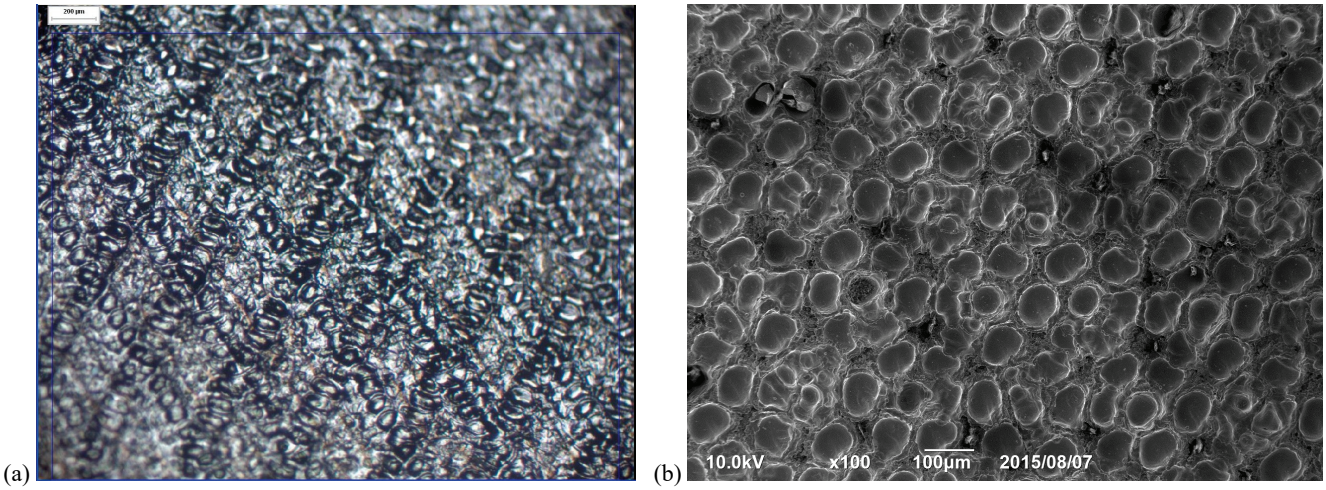

Fig. 2. (a) Optic micrograph of the laser pattern and (b) SEM view of laser treated Ti6Al4V surface before coating

2.3. Syntesizing of reduced nano-graphene oxide(rGO)

The reduced nano-graphene oxide (rGO) was syntesized using a modified Hummers method from the graphite powders by oxidation with $NaNO_3$, H_2SO_4 and $KMnO_4$ in an ice bath [16]. Briefly put, 100 mL of concentrated H_2SO_4 was added into a mixture of graphite flakes (3.3 g) and $NaNO_3$ (2.5 g). The mixture was cooled in an ice bath, and stirred for 30 min. $KMnO_4$ (15 g) was slowly added and stirred for another 30 min. The reaction was then warmed to 35 °C, and stirred for two more hours. Water (150 mL) was slowly added and then 30% H_2O_2 (15 mL). The mixture was stirred for an hour, filtered, washed with HCl:H_2O (1:10), and dried in vacuum furnace. Then, 15 mg rGO powders were processed in an ultrasonic bath until a dispersed brown-colored rGO powder flakes (approx. 200 nm) were obtained in aqueous solvents.

2.4. Hybrid sol-gel coating

Hydroxyapatite and other powders were received from commercial suppliers (Sigma-Aldrich). A designed amount of Hydroxyapatite (25 µm, Merck) was dissolved in deionized water to form a solution. The mixture was sealed in a glass beaker immediately and then stirred vigorously using a hot plate. Phosphoric pentoxide (P_2O_5) was dissolved in another portion of deionized water to form a solution and added dropwise into the hydroxyapatite solution. After that, potassium dihydrogen phosphate (KH_2PO_4) was subsequently added into the hydrolysed phosphorus sol and magnetic stirring was continued for an additional 30 min. The chemicals wt. % concentrations are presented in Table 2. The solutions were mixed in a Ca/P molar as an initially mixed precursor solution. The mixture was continuously stirred for about 1h at ambient temperature. As a result of this process, a white transparent sol was obtained. After that, the solution was ho-

mogenized using the ultrasonic homogenizer for about 15 min. Meanwhile, during the ultrasonic homogenizing, $NaCO_3$ were added. After a clear gel was obtained if was then aged at room temperature for 1h. Finally, it was dried/aged at 60 °C for 2 h in a furnace. The resultant gel is either transparent or translucent depending on the concentration of HA and other biocompatible chemicals such as P_2O_5 and $NaCO_3$. After that the obtained solution was homogenized using the ultrasonic homogenizer about 15 min and rGO powders were added into the sol. The rGO concentrations were prepared (0.5 and 1% wt.) and a clear solution was obtained and aged at room temperature for 15 min. Then, the prepared gel was dried/aged at 60 °C for 12 h in an oven.

After single-HA and rGO/HA gel preparations, the substrates were dip coated at average of 30 μm film thickness using a dip coater at 250 mm/min descending and ascending rates. Phase and coated samples dried at room temperature. After the coated titanium specimens were aged at room temperature for four hours and pre-dried at electrical oven at 80 °C for four hours then dried samples were placed into a sintering furnace (Protherm, 1400 °C). All the specimens were sintered in a vacuum atmosphere at 750 °C, 800 °C and 850 °C for 1 h at 5 °C/min rate and then the sintered samples were left in air for cooling down to ambient temperature. The effect of sintering temperature was analysed during surface investigation and characterized via XRD, Raman spectroscopy and Field Emission Scanning Electron Microscope/focused ion beam (FESEM).

Table 2. Concentration ratios used during the sol-gel process

$Ca_5(OH)(PO_4)_3$ [%]	P_2O_5 [%]	KH_2PO_4 [%]	Na_2CO_3 [%]	pH
50	15	5	30	7.8

2.5. Adhesion strength

Adhesion resistances of the coated samples between the substrate and the coating layer, and shear test was performed (Instron-8562). Adhesion tests were applied at 2 mm/min rates in accordance with the ASTM-C 633 standard. A compressive load (500 gr) was applied to both strips during the curing to ensure an intimate contact between resin and the two surfaces. After curing at 80 °C for 12 h in a furnace, the bonded strips were bench cooled to room temperature, then the pressure was released and the resin-bonded rods were removed from the device. Tensile test was applied on the surfaces that were joined with DP460 epoxy (3M) adhesive and the adhesion resistances were calculated by considering the joint surface areas and rupture force values. Then, the data were converted to adhesion resistance graphics with the help of data acquisition system software and were evaluated comparatively. Five specimens were used for each sample group and the mean values were considered during the experiments.

3. Results

Reduced nano-graphen oxide, rGO-reinforced HA film at average thickness (~2 nm) have been experimentally achieved on laser-treated Ti substrates. For this, different sols were prepared at various wt. % HA and rGO-HA comprising nano-sized pores. Raman spectroscopy was used to investigate the electronic structure of rGO and the reduction degree of rGO. The Raman spectra of rGO shown in Fig. 4a, b indicate that rGO possesses a D band at 1343 cm^{-1} and a G band at 1590 cm^{-1}. Such findings confirm that reduction degree of rGO increases when the ordered structure is restored. To evaluate the sintering temperature and rGO substitution effect on the surface morphology, three different sintering temperatures (750, 800 and 850 °C) were applied onto the single HA and HA/rGO composite coated specimens. Figure 5 shows the XRD patterns of the coated (HA and GO/HA) samples at different sintering temperatures (750, 800 and 850 °C). From the patterns, it can be clearly seen that the major peaks depict HA. The highest peak of a-tricalcium phosphate, TCP, can be seen in the same figure. The intensity of the XRD peaks increased without significant change in the XRD peak broadening, and this suggests that the crystallinity of the HA phase improved with increasing temperature, as expected. The changes in morphologies of the single HA-coated (Fig. 6a, b) and double HA/rGO-coated (Fig. 7a, b) samples were characterized by a (FIB) electron microscope (JEOL Dual Beam, JIB-4601F).

The surface structure of the laser-treated samples (2×2 μm) were analysed by SEM. Through the SEM analysis, it was shown that on the surfaces some cracks occurred after HA coating during sinterind and drying. The SEM micrographs, shown in Fig. 6a–b and Fig. 7a–c for the single-layer HA-coated and rGO-reinforced (HA/rGO) (1wt%) films obtained after single coating (~0.6 μm film thickness) on titanium alloys followed by thermal treatment at ~750 °C for 1 h. Throughout SEM investigations, the coating morphol-

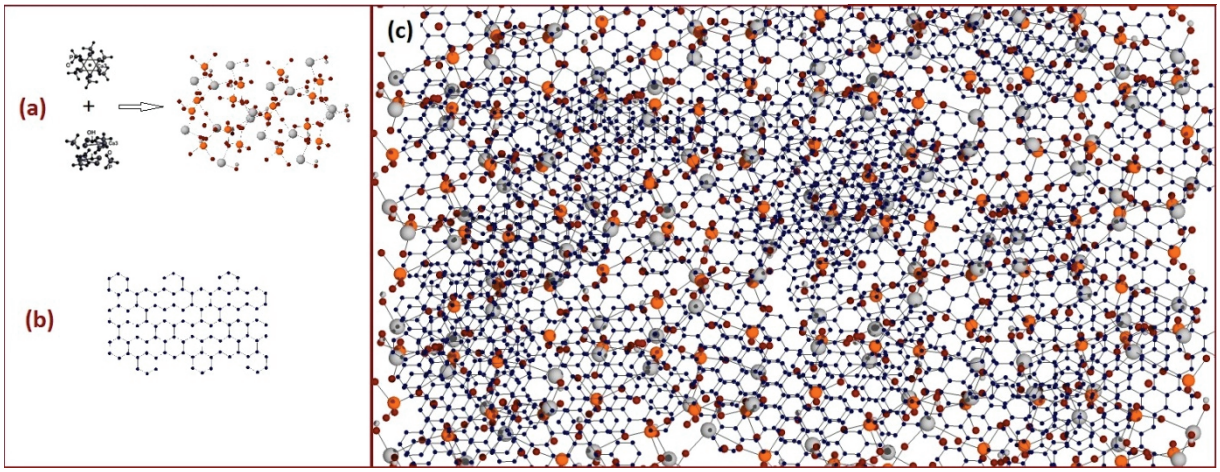

Fig. 3. Molecular visualization of GO, HA structure: (a) molecular structure of HA, (b) molecular structure of GO, (c) simulation of GO/HA structure

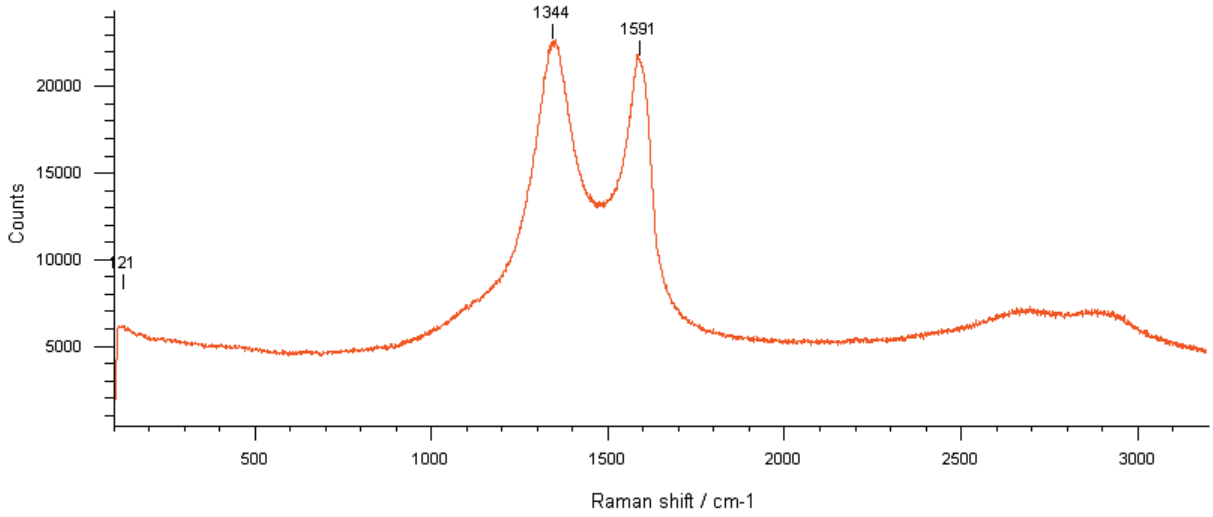

Fig. 4. Raman spectra of nGO peaks

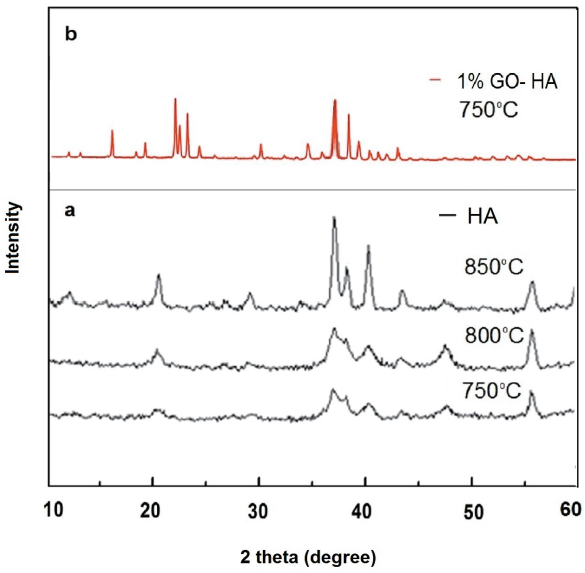

Fig. 5. XRD patterns of HA and 1% rGO-HA coatings

ogy appeared homogeneous, rough and containing pores having the average particle size of 275 nm. SEM images of rGO-HA double-layer coated surfaces showed uniform, homogeneous morphology without any cracks with no coating particles peeled off from the substrate, which could suggest the existence of a substantial cohesive strength between the particles. A smooth, dense and crack-free nanostructured rGO-HA film (~0.6 μm) with low porosity has been achieved at 750 °C sintering temperature in a controlled atmosphere.

A compressive load (500 g) was applied to both strips during curing to ensure an intimate contact between resin and the two surfaces. After curing at 80 °C for 12 h in a furnace, the bonded strips were bench cooled to room temperature, then the pressure was released and the resin bonded rods were removed from the device. The coating substrate bonding strength was measured using an Instron 8562 tester at a crosshead

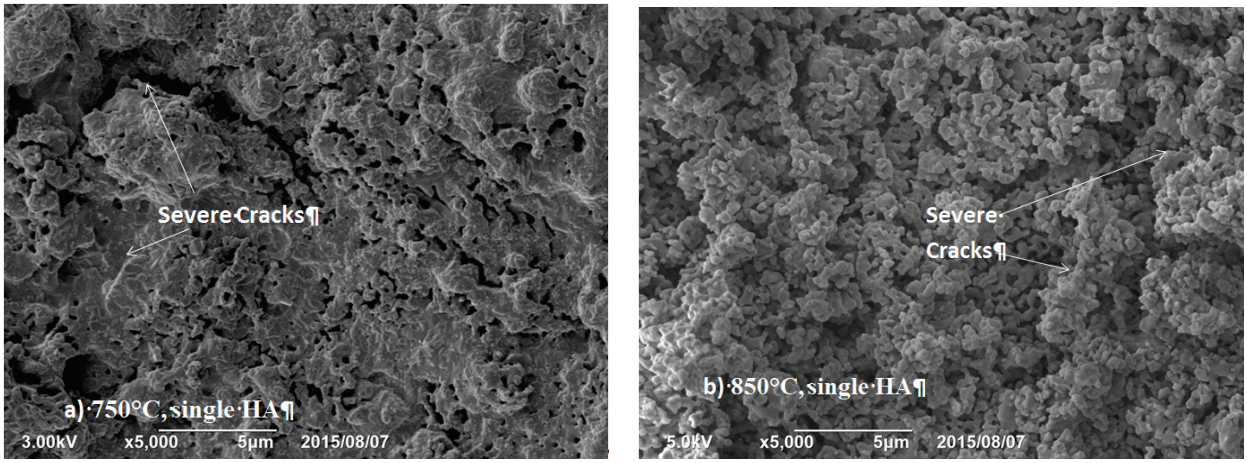

Fig. 6. FESEM images of Single-HA coated Ti6Al4V at (a) 750 °C and (b) 850 °C sintering temperatures

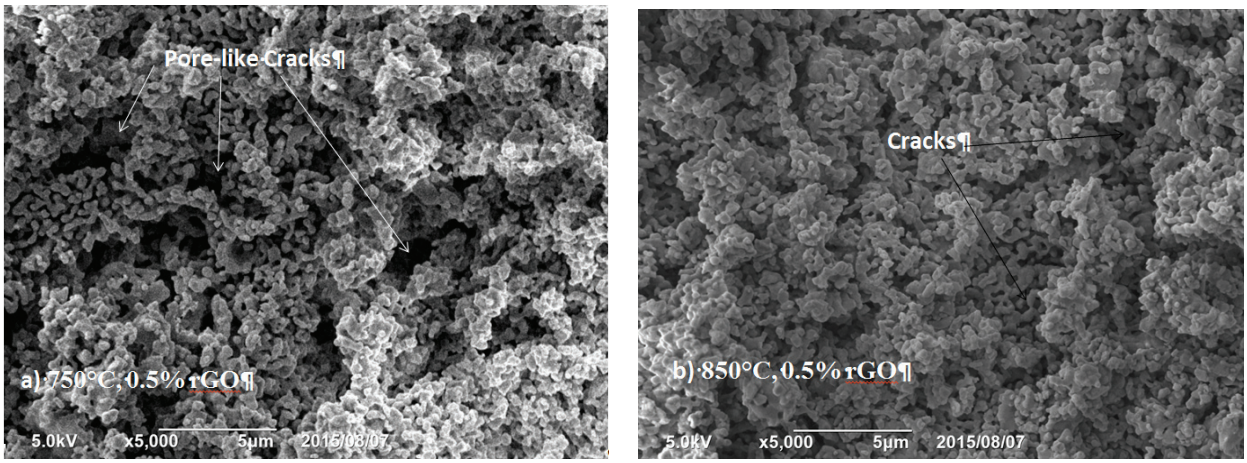

Fig. 7. FESEM images of Single-HA coated Ti6Al4V at (a) 750 °C and (b) 850 °C sintering temperatures

speed of 2.0 mm/min. Figure 9 shows the bonding strengths of the untreated, laser surface treated single HA-coated and rGO-substituted HA-coated substrates with 0.5, 1.0 and 1.5 wt. % rGO concentration rates. The adhesion strength of the single layer HA-coated samples with surface laser treated were found to be 10 MPa in average compared to the coatings with untreated surface to having only 6 MPa. However, the adhesion strengths of the rGO-reinforced (0.5% and 1.0%) HA coatings were found to be 11.0 MPa and 12.0 MPa in average, respectively.

4. Discussion

4.1. HA and rGO characterization

The Raman spectrum of rGO shown in Fig. 4a (for 0.5% rGO) and 4b (for 1.0% rGO), clearly show that the FWHM of D bands decrease upon the MWI duration, indicating the increase of highly oriented and multi-layered reduced nano graphene oxide, rGO. Based on the results, it could be indicated that the structure of rGO via the present method is expected to be dominated by the duration of MWI and the amount of the hydrazine hydrate solution used. They depict the presence of D, G and 2D peaks, in which G peak is from the in-plane C–C bond stretching in rGO, D peak is related to the defects in the structure, and 2D peak is associated with multi layered rGO structure. rGO sheets are mostly decorated with epoxide and hydroxyl groups, whereas the carboxyl groups are located at the edges and these oxygen-containing functional groups induce the subsequent formation of nanostructures attached on the surfaces and edges of rGO sheets. At the beginning of the hydrothermal reaction, Ca^{2+} can be absorbed on the rGO through the coordination interaction of the C–O–C and –OH groups (Fig. 4). Meanwhile, ion exchange may occur with H^{+} from carboxyl groups, thus resulting in the

formation of functional materials with various structures. Such hydrothermal method is an easy method for rGO/HA composite synthesis, meanwhile the process also controls the crystal morphology of the composite.

Phase constituents of the sintered samples were identified by X-ray diffraction using Cu Ka radiation, k = 1.54056A° XRD. The XRD pattern of rGO/HA powder, was shown in Fig. 5. It shows that the XRD patterns of sintered samples contain different amounts of graphene nano sheets (nsGO). It is clearly seen that the major peaks in the diffraction patterns correspond to HA. The highest peak of a-tri calcium phosphate (a-TCP) (2θ = 30.71°) overlaps with one peak of HA (2θ = 30.52°), the second highest peak of a-TCP (2θ = 22.89°) overlaps with one peak of HA (2θ = 22.96°), the third highest peak of a-TCP (2θ = 34.21°) is detected, but the peak height is not so evident in the sintered HA and 1.0 wt.% rGO composites. On the other hand, the three highest peaks of b-TCP, highest peak: 2θ = 30.9°, second highest peak: 2 h = 34.37° are evident but third highest peak: 2θ = 27.77° is absent. XRD analysis illustrates sufficiently that few dissociation of HA into b-TCP occurred due to the rapid processing conditions and low sintering temperature (850 °C) during vacuum sintering. It is also evident from XRD results that dissolution of calcium would be accelerated on the surface of the rGO/HA composite due to inhibition of HA grain growth by the additive rGO on the grain boundaries. Moreover, smaller grain size generally results in more specific area of the sample, which, in turn, benefits the interaction with body fluids and ultimately increases dissolution of calcium ions.

4.2. Coating

To show and compare the effect of rGO reinforcement at two different concentrations (0.5 and 1.0%) on surface morphology, the coated surfaces both by single-HA and rGO/HA biocomposites were analysed and SEM views were given in between Figs. 6 and 8. Figure 6a, b shows the surface morphology with severe cracky surfaces of the single-HA composite coated samples sintered at 750 °C (a) and 850 °C (b). The FESEM micrographs of the rGO reinforced rGO/HA coating films sintered at 750 °C (Fig. 7a) and 850 °C (Fig. 7b) show that the films exhibit better homogenous morphology with small pore-like cracky surfaces.

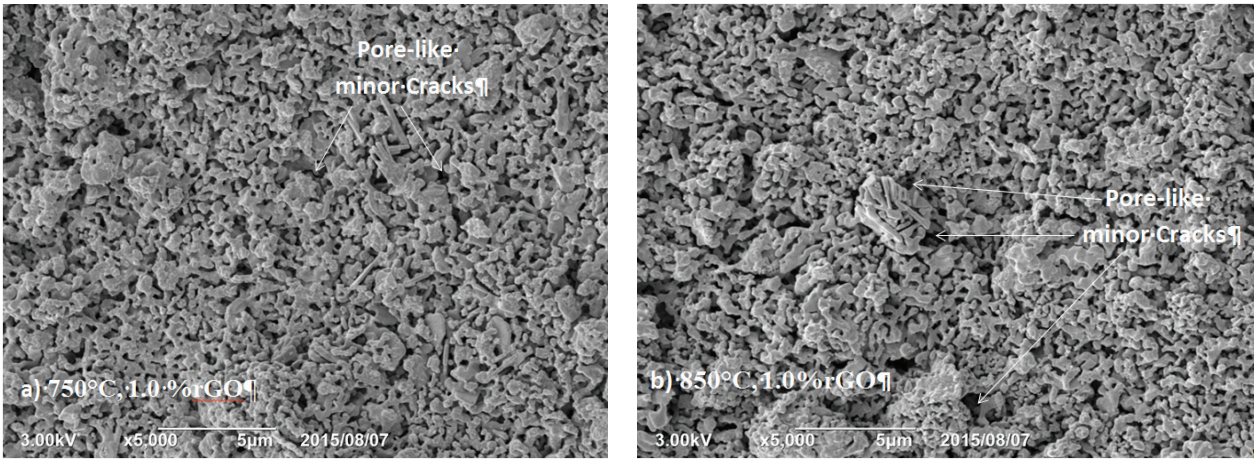

Fig. 8. FESEM images of rGO/HA coated Ti6Al4V at (a) sintered at 750 °C with 0.5% rGO substitution, (b) sintered at 850 °C with 0.5% rGO substitution

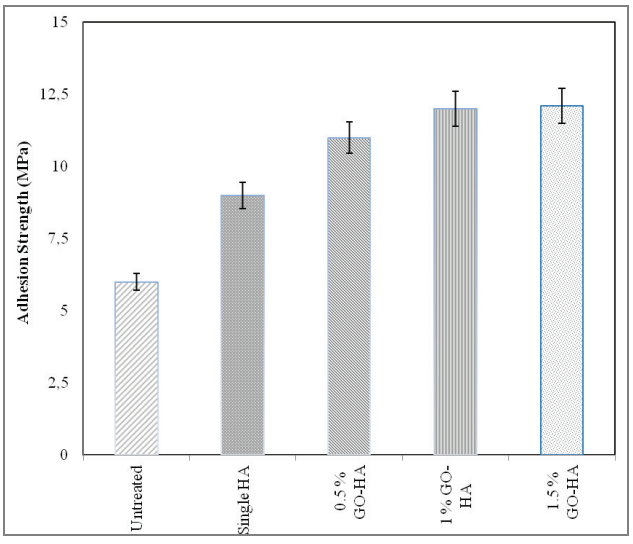

Fig. 9. Variation of adhesion strengths for HA and rGO/HA coated samples

As shown in Fig. 6a, b, SEM images of the single-HA coating at 750 °C and 850 °C, the coating surface is non-homogenous due to inadequate sintering temperature, and surface morphology exhibits severe cracks, probably due to the different thermal expansions and shrinkage occurring during the thermal process that could supply points of mechanical interlocking to promote osteointegration [9]. Thus, much higher temperature is required to achieve better crystallization of HA and higher density of the layer. For this reason rGO at various concentration rates (0.5 and 1.0%) was substituted into HA and the coated samples were sintered at the same temperatures. It appears that very fine particles of HA were sintered slightly during the sintering process based on the observed surface of the particles. Fig. 7a, b shows the surface morphologies of the rGO/HA coated samples. As shown in Fig. 7, better morphology and crystallization was obtained for the sample coated by rGO/HA biocomposite compared to the single-HA coated ones (Fig. 6a, b). The increase of sintering temperature leads to higher binding energies that can be correlated with the fact that the effective charge density on calcium and phosphorus cations increases.

It was found that the rGO reinforced HA at various (wt. %) concentrations provided better sinterability by observing much better interconnections between powders (Fig. 8). Such bonding is mostly desired due to bone growth with a bioactive surface that enables a direct bond between the implants and the surrounding bone, where the bioactivity is the ability of a material to attach itself to the living tissues without an interposing the tissue layer. The high specific surface area of rGO is capable of forming an increased contact area with matrix and SEM morphology investigation depicted that wrapping of a rGO around HA grain is clearly visible.

4.3. Adhesion strength

Adhesion strength of the coated Ti alloy with 1 wt. % rGO/HA samples was measured to have 12 MPa, on average. As shown in Fig. 9, the bonding strength of single-HA coating samples was 9 MPa on average. It was found that the bonding strength of 1 wt. % rGO--coated samples on the laser-textured surface is by about ~25% higher than the single-HA coatings at 850 °C sintering.

The higher adhesion strength of 1 wt. % rGO/HA specimen was attributed to the strength of rGO. Cracks observed on the coating surface (Fig. 6a, b) negatively affected the adhesion resistance of the single-layer HA coatings. The FESEM analyses showed that, due to better sintering and interconnection between HA and GO, a structure having pore-like cracks at low level as shown in Fig. 8a–b, produced high adhesion strength in both 0.5 and 1 wt% rGO/HA coatings (Fig. 9). In literature, it is also indicated that the surface cracks diminish the adhesion strength [9]. The reason of increased adhesion strength of the coatings is thought to be associated with the rate of rGO. It was shown that particularly the coatings with 1 wt. % rGO substituted coatings had a homogeneous surface morphology generated with very low pore-like cracks or free of coating cracks on the surface (Fig. 8a, b).

As a result, the bonding strength of rGO-reinforced samples were significantly enhanced, and more energy would be required to make the nanofiller pull-out from HA matrix. It can be concluded that, a rough and wrinkled surface texture coupled with low-surface cracks of the rGO (Fig. 7a–b) also plays an important role in enhancing mechanical interlocking, leading to increased load-transfer efficiency between HA matrix and rGO and, therefore, results in high adhesion strengths compared to untreated and single-HA-coated samples (Fig. 9). In addition, compared to untreated surface, the surface treatment enhanced the adhesion strength as much as 100% when coupled with rGO reinforcement. However, as shown in Fig. 9, it can be seen that the increased rGO rate up to 1.5% did not increase the adhesion strength (12.1 MPa). As it was reported and proven, for the orthopedic applications the minimum adhesion strength was between 7 and 10 MPa [29]. Such requirement was also indicated in a standard as per ISO 13779-2 standard for the HA coatings on bio-implants.

5. Conclusions

The novel rGO-reinforced HA biocomposite coatings on Ti6Al4V alloys with laser-modified surface were demonstrated using the sol gel method. Compared with the single layer-HA, the rGO/HA coatings produced more homogeneous and smooth surface morphology and also enhanced the adhesion strength between the sustrate and coating layer. Due to the high specific surface area of rGO, the adhesion (bonding) strength between the substrate and rGO/HA could be significantly enhanced.

The present investigations have shown that the both surface treatment and 1% rGO substitution into HA increased the adhesion strength by 25% and 100% compared to the single HA coatings and untreated-HA

coated samples, respectively. The best surface morphologies and high adhesion strength were obtained at 1% rGO/HA biocomposite coatings at 850 °C sintering temperature. It can be concluded that rGO reinforcement exhibits significant effect on morphology and bonding strength of HA + rGO biocomposite coatings. However, further *in vitro* and *in vivo* work on cell responses is certainly needed via the aqueous--based sols for better understanding of the benefits of the current coating processes.

Acknowledgements

This project was supported by Yildiz Technical University, BAPK (Grant No. 2015-07-YL-01). The authors give thanks to Dr. Meltem Sezen and Dr. Feray Bakan from Sabanci University-Nanotechnology Research &Application Centre for help in the analysis.

References

[1] AKHAVAN O., GHADERI E., *Toxicity of graphene and graphene oxide nanowalls against bacteria*, ACS Nano, 2010, 4, 5731–5736.

[2] BARADARAN S., MOGHADDAM E., BASIRUN W.J., MEHRALI M., SOOKHAKIAN M., HAMDI M. et al., *Mechanical properties and biomedical applications of a nanotube hydroxyapatite-reduced graphene oxide composite*, Carbon, 2014, 69, 32–45.

[3] BUSER D., SCHENK R.K., STEINMANN S., FIORELLINI J.P., FOX C.H., STICH H., *Influence of surface characteristics on bone integration of titanium implants a histomorphometric study in miniature pigs*, J. Biomed. Mater. Res., 1991, 25, 889–902.

[4] CHEN C.Z., TIAN Y.S, LI S.T., HUO Q.H., *Research progress on laser surface modification of titanium alloys*, Appl. Surf. Sci., 2005, 242, 177–184

[5] FAN Z., WANG J., WANG Z., RAN H., LI Y., NIU L. et al., *One-pot synthesis of graphene/hydroxyapatite nanorod composite for tissue engineering*, Carbon, 2014, 66, 407–416.

[6] FANG L., LENG Y., GAO P., *Processing and mechanical properties of HA/UHMWPE nanocomposites*, Biomaterials, 2006, 27(20), 3701–3707.

[7] FRANK I.W., TANENBAUM D.M., VAN DER ZANDE A.M., MCEUEN P.L., *Mechanical properties of suspended graphene sheets*, J. Vac. Sci. Technol. B, 2007, 25(6), 2558–2561.

[8] HU W.B., PENG C., LUO W. J., LI X., LI D., HUANG, Q., FAN C., *Graphene-based antibacterial paper*, ACS Nano, 2010, 4, 4317–4323.

[9] KUN P., TAPASZTO O., WEBER F., BALAZSI C., *Determination of structural and mechanical properties of multilayer graphene added silicon nitride-based composites*, Ceram. Int., 2012, 38(1), 211–216.

[10] LEE C., WEI X.D., KYSAR J.W., HONE J., *Measurement of the elastic properties and intrinsic strength of monolayer graphene*, Science, 2008, 321, 385–388.

[11] LI D., MULLER M.B., GILJE S., KANER R.B., WALLACE G.G., *Processable aqueous dispersions of graphene nanosheets*, Nat. Nanotechnol., 2008, 3(2),101–195.

[12] LAHIRI D., GHOSH S., AGARWAL A., *Carbon nanotube reinforced hydroxyapatite composite for orthopedic application: a review*. Mater. Sci. Eng., C 2012, 32(7), 1727–1758.

[13] LIU H., XI P., XIE G., SHI Y., HOU F., HUANG L. et al., *Simultaneous reduction and surface functionalization of graphene oxide for hydroxyapatite mineralization*, J. Phys, Chem. C, 2012,116(5), 3334–3341.

[14] LI M., WANG Y., LIU Q., LI Q., CHENG Y., ZHENG Y. et al., *In situ synthesis and biocompatibility of nano hydroxyapatite on pristine and chitosan functionalized graphene oxide*, J. Mater. Chem. B, 2013, 1(4), 475–484.

[15] LIU S.B., ZENG T.H., HOFMANN M., BURCOMBE E., WEI J., JIANG R., KONG J., CHEN Y., *Antibacterial activity of graphite, graphite oxide, graphene oxide, and reduced gra-phene oxide: membrane and oxidative stress*, ACS Nano, 2011, 5, 6971–6980.

[16] NAYAK T.R., ANDERSEN H., MAKAM V.S., KHAW C., BAE S., XU X. et al., *Graphene for controlled and accelerated osteogenic differentiation of human mesenchymal stem cells*, ACS Nano, 2011, 5(6), 4670–4678.

[17] RAFIEE M.A., RAFIEE J., WANG Z., SONG H.H., YU Z.Z., KORATKAR N., *Enhanced mechanical properties of nanocomposites at low graphene content*, ACS Nano, 2009, 3(12), 3884–3890

[18] SADAT S.M., KHORASANI M.T., DINPANAH K.E., JAMSHIDI A., *Synthesis methods for nanosized hydroxyapatite with diverse structures*, Acta Biomater., 2013, 9 (8),7591–7621.

[19] SAFFAR K.P., ARSHI A.R., JAMILPOUR N., NAJAFI A.R., ROUHI G., SUDA L., *A cross-linking model for estimating Young's modulus of artificial bone tissue grown on carbon nanotube scaffold*, J. Biomed. Mater. Res. A, 2010, 94A, 594–602.

[20] SAY Y., AKSAKAL B., *Effects of hydroxyapatite/Zr and bioglass/Zr coatings on morphology and corrosion behaviour of Rex-734 alloy*, J. of Mater. Sci: Mater. in Medicine, 2016, 27(6), 1–8.

[21] SAY Y., AKSAKAL B., DIKICI B., *Effect of hydroxyapatite/SiO_2 hybride coatings on surface morphology and corrosion resistance of REX-734 alloy*, Ceramics Int., 2016, 42(8), 10151–10158

[22] STEURER P., WISSERT R., THOMANN R., MUELHAUPT R., *Functionalized graphenes and thermoplastic nanocomposites based upon expanded graphite oxide*, Macromol. Rapid Commun., 2009, 30(4–5), 316–327.

[23] TUCKER B., COTTELL C., AUYEUNGT R., SPECTOR M., NANCOLLAS G., *Pre-conditioning and dual constant composition dissolution kinetics of pulsed laser deposited hydroxyapatite thin films on siliconsubstrates*, Biomaterials, 1996,17, 631–637.

[24] VALLES C., NUNEZ J.D., BENITO A.M., MASER W.K., *Flexible conductive graphene paper obtained by direct and gentle annealing of graphene oxide paper*, Carbon, 2012, 50(3), 835–844.

[25] VELAYUDHAN S., ANILKUMAR T.V., KUMARY T.V., MOHANAN P.V., FERNANDEZ A.C., VARMA H.K. et al., *Biological evaluation of apliable hydroxyapatite–ethylene vinyl acetate co-polymer composites intended for cranioplasty*, Acta Biomater., 2005, 1(2), 201–209.

[26] WHITE A.A., BEST S.M., KINLOCH I.A., *Hydroxyapatite--Carbon Nanotube Composites for Biomedical Applications: A Review*, Int. J. Appl. Ceramic Technol., 2007, 4(1), 1–13.

[27] XIAO Y., GONG T., ZHOU S., *The functionalization of multi-walled carbon nanotubes by in situ deposition of hydroxyapatite*, Biomaterials, 2010, 31(19), 5182–5190.

[28] ZHANG L., LIU W., YUE C., ZHANG T., LI P., XING Z. et al., *A tough graphene nanosheet/hydroxyapatite composite with improved in vitro biocompatibility*, Carbon, 2013, 61, 105–115.

[29] KUN P., TAPASZTO O., WEBER F., BALAZSI C., *Determination of structural and mechanical properties of multilayer graphene added silicon nitride-based composites*, Ceram. Int., 2012, 38(1), 211–216.